REPORT DOCUMENTATION PAGE

Form Approved OMB NO. 0704-0188

1. REPORT DATE (DD-MM-YYYY)	2. REPORT TYPE	3. DATES COVERED (From - To)
14-12-2015	Final Report	16-Jul-2012 - 15-Jul-2013

4. TITLE AND SUBTITLE
Acquisition of a Nanoindenter for Studying Mechanical Properties of Nanomaterials, Supporting Future Research in Robotics and Enhancing Research-related Education

5a. CONTRACT NUMBER
W911NF-12-1-0294

5b. GRANT NUMBER

5c. PROGRAM ELEMENT NUMBER
611103

6. AUTHORS
Mingjun Zhang

5d. PROJECT NUMBER

5e. TASK NUMBER

5f. WORK UNIT NUMBER

7. PERFORMING ORGANIZATION NAMES AND ADDRESSES
University of Tennessee at Knoxville
1534 White Avenue

Knoxville, TN 37996 -1529

8. PERFORMING ORGANIZATION REPORT NUMBER

9. SPONSORING/MONITORING AGENCY NAME(S) AND ADDRESS (ES)
U.S. Army Research Office
P.O. Box 12211
Research Triangle Park, NC 27709-2211

10. SPONSOR/MONITOR'S ACRONYM(S)
ARO

11. SPONSOR/MONITOR'S REPORT NUMBER(S)
61479-LS-RIP.12

12. DISTRIBUTION AVAILIBILITY STATEMENT
Approved for Public Release; Distribution Unlimited

13. SUPPLEMENTARY NOTES
The views, opinions and/or findings contained in this report are those of the author(s) and should not contrued as an official Department of the Army position, policy or decision, unless so designated by other documentation.

14. ABSTRACT
We propose to acquire a nanoindenter for nanoscale force measurement, and material property characterization. The instrument will be used to support research and education for our current ARO sponsored project. We will employ the instrument, and incorporate our AFM-confocal integrated system to systematically characterize mechanical properties of ivy nanoparticles. The experiences gained through this research will be used for future DoD projects.

15. SUBJECT TERMS
Nanoparticles, nanoindentation, nanomechanics, nano-scale mechanical properties

16. SECURITY CLASSIFICATION OF:			17. LIMITATION OF ABSTRACT	15. NUMBER OF PAGES	19a. NAME OF RESPONSIBLE PERSON
a. REPORT	b. ABSTRACT	c. THIS PAGE			Mingjun Zhang
UU	UU	UU	UU		19b. TELEPHONE NUMBER 614-292-3181

Report Title

Acquisition of a Nanoindenter for Studying Mechanical Properties of Nanomaterials, Supporting Future Research in Robotics and Enhancing Research-related Education

ABSTRACT

We propose to acquire a nanoindenter for nanoscale force measurement, and material property characterization. The instrument will be used to support research and education for our current ARO sponsored project. We will employ the instrument, and incorporate our AFM-confocal integrated system to systematically characterize mechanical properties of ivy nanoparticles. The experiences gained through this research will be used for future DoD projects.

The instrument will also be used to support our bio-inspired micro-robotics research, which is one of the active research themes in our lab. Our interest for the subject is on development of a bio-inspired swimming micro-robot. The nanoindenter will be used to characterize materials with similar properties to that of biological flagella, and contribute to the development of a prototype swimming micro-robot.

In addition, we will use the instrument to train post-doctoral researchers, graduate and undergraduate students.

We will also use the instrument for the following projects that may be potential interests for DoD's missions:

*. Bio-inspired high strength, fire resistant nanocomposite.
*. Bio-inspired nanocomposite adhesive.
*. Bio-inspired nanomaterials for tissue engineering.
*. Bio-inspired micro-robotics.

In summary, the aims of this instrument are:

Aim One: To advance research on characterizing mechanical properties of nanoparticles, compare the results with AFM analysis, and provide an in-depth comprehensive view on mechanics of the ivy nanoparticles.

Aim Two: To combine the nanoindenter with an AFM/confocal integrated system, and characterize mechanical properties of nanomaterials for future DoD projects.

Aim Three: To employ the nanoindenter for characterizing material properties of flagella in Giardia, and materials used to develop a prototype swimming micro-robot.

Aim Four: To educate students carrying on independent research in the emerging field of nanotechnology.

Enter List of papers submitted or published that acknowledge ARO support from the start of the project to the date of this printing. List the papers, including journal references, in the following categories:

(a) Papers published in peer-reviewed journals (N/A for none)

Received		Paper
12/06/2015	3.00	Yongzhong Wang, Leming Sun, Sijia Yi, Yujian Huang, Scott C. Lenaghan, Mingjun Zhang. Naturally Occurring Nanoparticles from, Advanced Functional Materials, (05 2013): 2175. doi: 10.1002/adfm.201202619
12/06/2015	4.00	Lijin Xia, Zhonghua Xu, Leming Sun, Patrick M. Caveney, Mingjun Zhang. Nano-fillers to tune Young's modulus of silicone matrix, Journal of Nanoparticle Research, (03 2013): 1388. doi: 10.1007/s11051-013-1570-0
12/06/2015	6.00	Jason N Burris, C Neal Jr Stewart, Mingjun Zhang, Yujian Huang, Scott C Lenaghan, Lijin Xia. Characterization of physicochemical properties of ivy nanoparticles for cosmetic application, Journal of Nanobiotechnology, (02 2013): 1. doi: 10.1186/1477-3155-11-3
12/06/2015	7.00	B. Lady, S. C. Lenaghan, J. N. Burris, K. Chourey, Y. Huang, L. Xia, R. Sharma, C. Pan, Z. LeJeune, S. Foister, R. L. Hettich, C. N. Stewart, M. Zhang. Isolation and chemical analysis of nanoparticles from English ivy (Hedera helix L.), Journal of the Royal Society Interface, (07 2013): 1. doi: 10.1098/rsif.2013.0392
12/06/2015	8.00	Sijia Yi, Yongzhong Wang, Yujian Huang, Lijin Xia, Leming Sun, Scott C. Lenaghan, Mingjun Zhang. Tea Nanoparticles for Immunostimulation and Chemo-Drug Delivery in Cancer Treatment, Journal of Biomedical Nanotechnology, (06 2014): 1016. doi: 10.1166/jbn.2014.1782
12/06/2015	9.00	Yongzhong Wang, Sijia Yi, Leming Sun, Yujian Huang, Scott C. Lenaghan, Mingjun Zhang. Doxorubicin-Loaded Cyclic Peptide Nanotube Bundles Overcome Chemoresistance in Breast Cancer Cells, Journal of Biomedical Nanotechnology, (03 2014): 445. doi: 10.1166/jbn.2014.1724
12/06/2015	10.00	Leming Sun, Sijia Yi, Yongzhong Wang, Kang Pan, Qixin Zhong, Mingjun Zhang. A bio-inspired approach for in situ synthesis of tunable adhesive, Bioinspiration & Biomimetics, (03 2014): 1. doi: 10.1088/1748-3182/9/1/016005
TOTAL:		**7**

Number of Papers published in peer-reviewed journals:

(b) Papers published in non-peer-reviewed journals (N/A for none)

Received Paper

TOTAL:

Number of Papers published in non peer-reviewed journals:

(c) Presentations

Number of Presentations: 0.00

Non Peer-Reviewed Conference Proceeding publications (other than abstracts):

Received Paper

TOTAL:

Number of Non Peer-Reviewed Conference Proceeding publications (other than abstracts):

Peer-Reviewed Conference Proceeding publications (other than abstracts):

Received Paper

TOTAL:

Number of Peer-Reviewed Conference Proceeding publications (other than abstracts):

(d) Manuscripts

Received		Paper
08/27/2013	1.00	Leming Sun, Sijia Yi, Yongzhong Wang, Kang Pan, Qixin Zhong, Mingjun Zhang. A Bio-inspired Approach for In Situ Synthesis of Tunable Adhesive, Bioinspiration & Biomimetics (07 2013)
12/13/2015	11.00	Yujian Huang, Yongzhong Wang, Li Tand, Leming Sun, Mei-Zhen Cu, Feng Hao, Mingjun Zhang. Nano-spherical Arabinogalactan Protein: A Key Component in the High-strength Adhesive Secreted by English Ivy, PNAS (12 2015)
TOTAL:		**2**

Number of Manuscripts:

Books

Received	Book
TOTAL:	

Received	Book Chapter
TOTAL:	

Patents Submitted

Patents Awarded

Awards

2013 Research Fellow Award (Faculty Award of Excellence in Research), College of Engineering, The University of Tennessee, Knoxville.

2012 Featured in the faculty appreciation week by students. One of the two faculty members elected from the College of Engineering for committing excellent teaching and research. The University of Tennessee.

Graduate Students

NAME	PERCENT_SUPPORTED	Discipline
Leming Sun	0.00	
Ben Reese	0.00	
Laura Yi	0.00	
Yujian Huang	0.00	
Stefan Nwandu-Vincent	0.00	
FTE Equivalent:	**0.00**	
Total Number:	**5**	

Names of Post Doctorates

NAME	PERCENT_SUPPORTED
Scott Lenaghan	0.00
FTE Equivalent:	**0.00**
Total Number:	**1**

Names of Faculty Supported

NAME	PERCENT_SUPPORTED
FTE Equivalent:	
Total Number:	

Names of Under Graduate students supported

NAME	PERCENT_SUPPORTED
FTE Equivalent:	
Total Number:	

Student Metrics

This section only applies to graduating undergraduates supported by this agreement in this reporting period

The number of undergraduates funded by this agreement who graduated during this period:	2.00
The number of undergraduates funded by this agreement who graduated during this period with a degree in science, mathematics, engineering, or technology fields:	0.00
The number of undergraduates funded by your agreement who graduated during this period and will continue to pursue a graduate or Ph.D. degree in science, mathematics, engineering, or technology fields:	0.00
Number of graduating undergraduates who achieved a 3.5 GPA to 4.0 (4.0 max scale):	0.00
Number of graduating undergraduates funded by a DoD funded Center of Excellence grant for Education, Research and Engineering:	0.00
The number of undergraduates funded by your agreement who graduated during this period and intend to work for the Department of Defense	0.00
The number of undergraduates funded by your agreement who graduated during this period and will receive scholarships or fellowships for further studies in science, mathematics, engineering or technology fields:	0.00

Names of Personnel receiving masters degrees

NAME
Total Number:

Names of personnel receiving PHDs

NAME	
Ben Reese	
Stefan Nwandu-Vincent	
Laura Yi	
Total Number:	**3**

Names of other research staff

NAME	PERCENT_SUPPORTED
FTE Equivalent:	
Total Number:	

Sub Contractors (DD882)

Inventions (DD882)

Scientific Progress

FINAL REPORT
==========

I. All items of equipment actually acquired

MFP-3D-SA AFM-based Nanoindenter and Components: $168,521.00
Manufacture: Asylum Research, an Oxford Instruments Company. Santa Barbara, CA 93117, United States.

MFP-3D-SA AFM-based Nanoindenter List price: $104,343.00
Includes nanoindentation and Piezoresponse Force Microscopy (PFM) detailed as following:

MFP-3D Head
Sensored optical lever with diffraction limited optics
Flexure-mounted optical lever system with low-coherence SLD, liquid-compatible and AC-capable cantilever holder, dichroic mirror and window for optical access to cantilever, 80-pitch engage screws, and Invar shell.
Noise: <0.02nm Adev in a 0.1Hz to 1kHz BW.
a low coherence light source
The NPS™ sensored Z axis provides precise measurements of the cantilever position for accurate force and topography measurements

MFP-3D XY Scanner
A flexured scanner and NPS sensors measuring the exact position of each axis (X-Y).
Scan Axes X&Y: 90µm travel in closed loop.
Closed loop position control with sensor noise <0.5nm average deviation (Adev) in a 0.1Hz-1kHz bandwidth (BW) and sensor nonlinearity <0.05% (Adev/full travel) at full scan.
Z: >15µm sensored travel. Sensor noise <0.25nm Adev in a 0.1Hz-1kHz BW and sensor non-linearity less than 0.05% (Adev/full travel) at full scan.
Z height: noise <0.06nm Adev, 0.1Hz-1kHz BW.
X, Y, & Z High Voltage Outputs: -10 to +150V.

MFP-3D Base
Three configurations for illuminating and viewing, i.e. top view, bottom view, and dual view.

All-Digital ARC2™ Controller List price: $64,178.00
100% digital for low noise, fast operation, and flexibility
Field Programmable Gate Array (FPGA) and Digital Signal Processor (DSP)
Fast analog-to-digital/digital-to-analog conversions
Digital Q-control: for cantilevers from 2kHz to 2MHz; typically enhances or suppresses Q by 5X.
DSP: Floating point processor running at 80MHz.
ADCs: One 16-bit input operating at 5MHz with seven gains and a 16-bit offset.
Five 16-bit inputs operating at 100kHz.
Frequency Synthesizer: Outputs from two Direct Digital Synthesizers (DDS) are are summed and available on a 16-bit, 10MHz DAC.
Frequency: DC to 2.0MHz in 2mHz increments.
Amplitude: 0 to 20V(p-p) in 0.6mV increments. Amplitude, phase, and frequency of the oscillator can be controlled from software at 100kHz update rates.
DACs: Six high resolution, ultra low-noise, fast 24-bit channels updated at 100kHz: two for XY scanning (14kHz bandwidth); one for Z feedback (117kHz bandwidth); and three general purpose (56kHz bandwidth).
Digital Lock-ins: The 5MHz ADC is the input to two fully digital lock-ins that provide quadrature outputs. Both R/¿ (amplitude/phase) and I/Q (Rcos¿/ Rsin¿) are available in output bandwidths up to 9kHz.

Total Cost of the System: $168,521

II. Research projects on which the equipment has been used

1. Identification of the chemical constituents of the ivy nanoparticles for unlocking the molecular basis for the ivy-derive high-strength adhesive (Army Research Office)

ACCOMPLISHED AIM ONE: Biomechanical properties of the ivy nanoparticles evaluated by the AFM-based nanoindenter.

By means of AFM and nanoindenter, abundant spherical organic nanoparticles have been observed in the secretions derived from the root hairs of English ivy (Fig. 1A). In particular, these proteinaceous nanoparticles are validated to exert crucial roles in

facilitating the attachment of the adventitious roots and favoring the climbing of English ivy. To massively harvest the ivy-derived nanoparticles, a platform for cost-effective cultivation of English ivy (H. helix) has been developed. This in vitro cultivation system not only raises the yield of the adventitious roots and the ivy nanoparticles, but it also maintains the adsorptive feature of the English ivy toward substrates. Uniform and spheroidal organic nanoparticles were obtained after isolation and purification using a size-exclusion high-performance liquid chromatography (SEC-HPLC) (Fig. 1C). As shown in Fig. 1B, the size of the purified ivy nanoparticles was approximately 70 nm in diameter, as measured by AFM. Comparatively, in aqueous suspension, the hydrodynamic size of these nanoparticles was 109.6 ± 2.3 nm (Fig. 1E), with a negatively charged surface at pH 7.0 (zeta potential = -29.0 ± 1.3 mV) (Fig. 1D), as characterized by dynamic light scattering (DLS) and electrophoretic light scattering (ELS). We further evidenced that these nanoparticles are predominantly composed of arabinogalactan proteins (AGPs), a superfamily of hydroxyproline-rich glycoproteins present in the extracellular spaces of plant cell. In order to test if or not AGPs are contained in the ivy nanoparticles, Yariv phenylglycoside dye, a reagent also called ß-glucosyl Yariv (ß-GlcY), which selectively binds to the AGPs via recognizing both given protein moieties and ß-1, 3-galactan chains with greater than five residues 1-3, was applied for the detection. As shown in Fig. 2A, characteristic AGP-like smeared bands in a high MW range were observed on respective SDS-PAGE gels stained with either Coomassie brilliant blue or 0.2% (w/v) ß-GlcY dye 4. Consistent with the gel information, the presence of AGPs in the purified ivy nanoparticles was further evidenced by Western blotting analysis using two monoclonal antibodies (mAbs), JIM 13 and JIM 14, which specifically recognize glycan epitopes of typical AGPs, as shown in Fig. 2B-F. In addition, Fourier transform infrared (FTIR) spectroscopic measurements indirectly validated the existence of AGPs in the ivy nanoparticles, in comparison the IR spectra of the ivy nanoparticles with those of a standard reference AGP, gum arabic. Furthermore, it was also observed that the ivy nanoparticles exhibited similar photoelectron spectra to the gum arabic, as measured by X-ray photoelectron spectroscopy (XPS). All the information described above demonstrates that the AGPs exist, at least partially, in the purified ivy nanoparticles. The spheroidal shape of the AGP-rich ivy nanoparticles results in a low viscosity of the ivy adhesive, and thus a favorable wetting behavior on the surface of substrates. Meanwhile, Ca2+-mediated association between carboxyl groups within AGPs and pectin gives rise to the cross-linking of the secreted adhesive, favors subsequent curing (hardening) via forming an adhesive film, and eventually promotes the generation of mechanical interlocking between the adventitious roots of English ivy and the surface of substrates.

ACCOMPLISHED AIM TWO: Combination of AFM and nanoindenter to characterize mechanical properties ivy adhesive for the construction of ivy-inspired adhesive.

In addition to the rich spherical nanoparticles observed in the periphery of the imprints of the root hairs, a translucent gel-like porous network comprising tightly cross-linked spheres in nanoscale was also detected in the adhesive remnant on the silicon wafers by SEM. To determine the chemical constituents of this matrix, the remnant substances exuded from the adventitious roots on the silicon wafers were re-suspended in PBS and examined using ELISA screening test, with 38 mAbs raised against the vast majority of the polysaccharides present in the plant cell wall. Accompanied by arabinogalactans, diverse pectic epitopes are also richly distributed in the adhesive secretions. Moreover, subsequent glycosyl composition assay identified that 4.09% (mol%) GalAp residues were contained in the adhesive substances recovered from the remnant on the silicon wafersfurther suggesting the existence of pectin in the mucilage derived from the adventitious roots of English ivy. Given that the arabinogalactans and pectic polysaccharides have been identified to be two of the predominant components in the majority of botanic adhesives, including those obtained from the climbing organs of Virginia creeper, Boston ivy, and Ficus pumila, as shown in the previous cytochemical analyses, it is logical to expect that these two acidic polysaccharides possess exceptional capacity to effectively support the adhesive function of the sticky exudates at the interface. In particular, for the mucilage secreted by the root hairs of English ivy, the pectic acids may exist alone and/or be covalently bonded to the AGPs within the ivy nanoparticles as interpreted above. More evidence regarding the co-existence of the AGPs and the pectic polysaccharides within the extracellular matrix of ivy root cells was obtained from the subsequent immunehistochemical assessment, further implying the functional correlations between these two components. Kevin C. Vaughn et al. have appropriately described the pectins and the AGPs in the botanic adhesive as “mucilaginous molecules that are spread across the surface of the structure to be attached, filling in the gaps”. In particular, “arabinans and AGPs appear to be an even more mobile component of the adhesive, filling in spaces between the papillate epidermal cells and even moving into small cracks in the structure that is attached”. In this respect, the effort in the exploration of the potential interactions among these acidic polysaccharides/glycoproteins may substantially improve our understanding of the molecular events controlling the generation of strong adhesion force within the ivy-derived bioadhesive. For such a purpose, a dot blotting test and a fluorescent combination assay were carried out to evaluate the hypothetical binding between the AGP-rich ivy nanoparticles and the pectic polysaccharides, apart from the aforementioned covalent connections of the AGPs and the pectic fraction within the ivy nanoparticles. To preliminarily assess the potential interactions using dot blotting, 20-34% esterified commercial pectin extracted from citrus fruit was dried down on PVDF membrane and subsequently incubated, after blocking, with the suspension of the purified ivy nanoparticles in the presence of 2 mM Ca2+. The level of the AGP-rich nanoparticles to which pectin bound was assessed by sequential incubation with JIM 13 primary antibody and HRP-conjugated secondary antibody. While the AGP-rich ivy nanoparticles indeed demonstrated concentration-dependent interactions with the adsorbed pectic polysaccharides, this combination was susceptible to the addition of external Ca2+-chelating agent, EGTA, which apparently suppressed the affinity of these two components. Additionally, this electrostatic interaction was further quantitatively evaluated using a fluorescent combination assay. Similar to the dot blotting examination, the pectic polysaccharides with a methyl esterification degree of 20-30% were coated onto 96-well plates prior to the blocking, and the Ca2+-containing suspension of the FITC-labeled ivy

nanoparticles was subsequently applied to each well. After 1 h incubation, the reaction buffer was removed and replaced with TBS, and the amount of the AGP-rich nanoparticles arrested by the adsorbed pectin was quantitatively determined by capturing the fluorescent intensity using plate reader. As expected, the concentration-dependent interactions between the ivy nanoparticles and the pectic polysaccharides was consistently observed in this assay. In the meanwhile, for the ivy nanoparticles tested with an initial concentration of 5 mg/ml, the amounts of the immobilized ivy nanoparticles detected in the incubation buffers containing 2 mM Ca2+ were approximately 2.1- to 2.5-fold and 1.5- to 1.8-fold greater than those of the nanoparticles remnant in Ca2+-free buffers and EGTA-containing buffers, respectively, at pectin concentrations ranging from 1 to 10 mg/ml, suggesting that the calcium ions are capable of promoting the electrostatic connections of the AGP-rich ivy nanoparticles and the pectin. To further validate this Ca2+-dependent interaction, 1 mg/ml ivy nanoparticles was applied to the combination assay under the same condition. In comparison to the respective amounts of the ivy nanoparticles retained by the adsorbed pectic polysaccharides in the absence of calcium ions and in the presence of excess EGTA, at least 2.0- and 1.2-fold greater amount of the FITC-conjugated nanoparticles was detected to be bound to the pectin in the EGTA-free reaction buffer containing 2 mM Ca2+. In addition, this Ca2+-modulated electrostatic interaction between the AGP-rich ivy nanoparticles and the pectic polysaccharides upon binding was further evidenced by testing the affinity of the AGP-rich ivy nanoparticles toward other electroneutral molecules, including BSA and fully esterified pectin, in the same assay. In contrast to the case containing 2 mM Ca2+, significant difference in the amount of the FITC-conjugated nanoparticles adsorbed after 1 h incubation was not observed in response to either the absence of calcium ions or the presence of external EGTA, indicating that the calcium ion-driven interaction between the AGP-rich ivy nanoparticles and the acidic pectic polysaccharides is the predominant force aiding in their combination. This electrostatic interaction is presumably displayed by calcium ions in facilitating the cross-linking among carboxyl groups of the uronic acid residues within the AGPs and the pectin. It is noteworthy that this Ca2+-driven event has been frequently discussed in the earlier reports, with experimental results consistent with that of the current study. Meanwhile, given that the Ca2+ is one of the richest and physiologically vital ions present in the extracellular space of plant cell, it is reasonable to conclude here that the Ca2+-regulated cross-linking among these acidic polysaccharides/glycoproteins undoubtedly renders potent driving force, effectively promoting the curing (hardening) progress of the sticky exudate derived from the adventitious roots of English ivy. In particular, under the natural condition, AGPs have shown a trend in raising the porosity of the native pectic gel, functioning as “pectin plasticizers” as described previously. In this respect, it seems reasonable to propose that in the ivy-derived adhesive, uronic acid-rich AGPs and pectic polysaccharides may cross-link to form a porous network upon hardening, an architecture shown in the SEM investigation as mentioned above. In light of the information gained from the overall study, the molecular basis for the ivy-derived adhesive at the interface is envisaged and summarized as following. Initially, for the attachment, the AGP-rich ivy nanoparticles are secreted toward the extracellular space of root cell upon contact with corresponding substrates in a manner that has been real-time monitored in our recent study. These spheroidal nanoparticles are concentrated during evaporation and the highly structural flexibility of the protein backbone as well as the anchored bulky AG branches of the AGPs allows these macromolecules to be tightly packed, reaching an intimate connection between adjacent nanoparticles. Subsequent Ca2+-driven cross-linking among carboxyl groups of the uronic acid residues within the AGPs and the pectic acids in the extracellular space favors the cohesion of the adjacent AGP-rich nanoparticles, gives rise to the generation of an adhesive film , further aids in the curing progress of the exuded adhesive, and thus realizes the adhesive function at the interface by restraining the relative movement of the adventitious roots and the corresponding substrates. Throughout these procedures, the AGP-rich ivy nanoparticles also possess the capacity to permeate into irregularities on the substrates owing to their rough surfaces in most cases, resulting in strong mechanical interlocking at the interface and further ensuring an ideal adhesive action.

The manner in which nano-sized particles are involved in the formation of an adhesive film between two adherends has been well elucidated in the case of the poly(vinyl acetate) adhesive, which is a conventional glue prepared via emulsion polymerization. Typically, commercially available poly(vinyl acetate) glues are comprised of synthetic particles in nanoscale dispersed in aqueous suspension. After being applied to a substrate, a three-step strategy was employed by this glue to accomplish adhesive activity at the interface, i.e. (i) tight packing of the particles upon evaporation, (ii) deformation of the particles toward intimate interactions, and (iii) coalescence (cross-linking) between adjacent particles to create a cohesively strong solid. Analogously, these engineered synthetic nanoparticles boost the mechanical interlocking of the glue at the interface in a similar pattern to the spheroidal nanoparticles observed in the ivy-derived adhesive, as documented in the previous reports. In this respect, in contrast to the consecutive molecular events in which the AGP-rich ivy nanoparticles involved as detailed above, it is logical to propose here that these two types of polymeric nanoparticles presumably share considerable mutual principles underlying their respective adhesive activities.

ACCOMPLISHED AIM THREE: Application of the AFM-based nanoindenter for characterizing the adhesive action of the engineered biomimetic and bioinspired adhesives.

In light of the uncovered molecular basis for the ivy-derived bioadhesive, a reconstructed biomimetic adhesive was subsequently developed by integrating the purified ivy nanoparticles with pectin in the presence of 2 mM calcium ions, to offer an engineering instance that might further evidence the putative adhesion mechanisms summarized above.

To precisely evaluate the behavior of the prepared adhesive, the adhesion force of this reconstructed adhesive was examined by a lap shear test, an approach that has been extensively applied to quantitatively assess bio-adhesives (Fig. 3A) 5-7. The

variation in shear forces of the prepared adhesive constructs was monitored over time to reflect the curing progress. As shown in Fig. 3B, in general, the shear force at failure of the ivy-mimetic composites was elevated with ascending in time and reached a plateau of maximum adhesion force in less than three days. To explore the specific roles of each component within the developed material, the shear forces of the Ca2+-free and EGTA-containing adhesive constructs were also traced throughout the test under the same condition. Similarly, the maximal shear forces of respective control groups could not be approached until approximately three days. However, significant difference in the shear force values that could be reached after three days was observed among distinct adhesive composites. At day 7, a shear force up to 341 ± 21.3 N was achieved by the ivy-mimetic adhesive construct prepared in the presence of Ca2+ and in the absence of EGTA, substantially greater than those of the Ca2+-free or EGTA-containing counterparts, with respective shear forces of ~ 201 ± 6.8 and 256 ± 28.6 N, indicating the significance of the calcium ions in developing an ivy-mimetic adhesive composite with expected level of performance. In addition to the apparent effects of the ionic strength, the influence of pH value on the adhesion force of the reconstructed ivy-mimetic adhesive was also evaluated by preparing the adhesive composites at distinct pH. As shown in Fig. 3C, in comparison to that of the adhesive composite prepared under neutral condition, slightly but significantly weaker shear forces obtained at day 7 were observed in response to the pH variations. In particular, in contrast to the composite developed in TBS at pH 7.6, approximately 1.4- to 1.5-fold lower adhesion forces were reached by the cases prepared at pH 4 or 9 after 7 days. Given that the cross-linking extent of the ivy-mimetic adhesive constructs is determined by the calcium-modulated electrostatic interaction which is susceptible to the pH variations, it is reasonable to expect this pH-responsive event here. This ivy-mimetic adhesive composite not only serves as an instance to support the proposed molecular basis for the ivy adhesive, but also affords a promising template for guiding the development of ivy-derived and ivy-inspired high-strength adhesive materials in the future.

ACCOMPLISHED AIM FOUR: Educational training.

In addition, several undergraduate/graduate students as well as some postdocs have been trained to use this AFM-base nanoindentation tool to advance relevant research.

2. Comparison of the Structure and Resulting Propulsion of Prokaryotic and Eukaryotic Flagella (Office of Naval Research)

This AFM-based nanoindenter has also been applied for characterizing material properties of flagella during the swimming motion. At present, no experimental studies have been conducted comparing the mechanical properties of flagella from prokaryotes and eukaryotes. While many theoretical studies have attempted to ascertain properties, such as Young's modulus and sheer modulus, the values from these theoretical studies are highly variable 8. Considering that accurate measurements of bending stiffness and elasticity are necessary for the development of more effective models of the fluid dynamics associated with flagella beating and propulsion, it is essential that these values be obtained. In addition to this need, by using nanoindentation, it will be possible to obtain these mechanical properties along the entire length of the flagella, indicating if different mechanical properties exist between different regions along the flagella, such as the hook region and basal body.

Specifically related to the mechanobiology of flagella, the PI's have collected preliminary data on the analysis of the flagella in T. foetus. Using an Asylum MFP/3D AFM housed in the PI's lab, scans were conducted to image T. foetus, and determine the position of the flagella. As shown in Fig. 4A, fixation and dehydration, followed by critical point drying, was effective at maintaining the shape and integrity of the flagella. Upon identifying the location of the flagella, force curves were conducted at various points along the flagella, and bare glass to obtain a value for the elastic modulus of these structures (Fig. 4A, inset). Based on these force curves, the modulus of glass was found to be ~70 GPa, in accordance with known values, while the modulus of the flagella was ~5 GPa (Fig. 4B-C). These preliminary experiments were conducted with a standard AFM cantilever, and thus the modulus may not be exact, due to the non-uniform shape of the tip. In addition to the data obtained from these experiments, force mapping was conducted on flagella to determine the apparent modulus of the flagella along their entire length. From these experiments, it was observed that the modulus was consistent along the length of the flagella, which was expected due to the repeating sub-units composing the structure. It is expected that in other flagella, the modulus may vary along the length, with the addition of secondary elements. These initial results validate the PI's approach and expertise, and demonstrate proof-of-concept for the proposed work with AFM. Considering the modular nature of the MFP/3D Nanoindenter proposed for use in this work, the methods developed and validated using the AFM will be similar to those validated in this preliminary work.

III. Research projects on which the equipment will be used

1. Quantifying Nano-mechanics and Nano-morphology of Cerebrospinal Fluid Components to Explore Association of TBI and AD (DoD FY15 PRARP Convergence Science Research Award)

We also propose to apply this AFM-based nanoindenter to characterize nanomechanical properties in our future projects. Specifically, the goal of our proposed research is to develop a nanotechnology approach for quantifying the effects of nano-mechanics for AD relevant to TBI in cellular level, which may provide direct evidence for understanding the association between TBI and AD. The uniqueness of this work lies in its synergetic integration of molecular mechanobiology and neuropathophysiology using a combined nano-instrumentation platform and quantitative multi-variable analysis approach for

nano-components isolated from cerebrospinal fluid components (CSF). This research may broadly impact the military, Veteran, and civilian communities by introducing significant benefits for characterizing effects of mechanics from TBI to AD, and providing an quantitative approach for diagnosing as well as predicting AD progress, and establishing the long-term consequences of TBI as they pertain to AD with mechanics evidence occurred at the cellular level. It meets the intent of the CSRA mechanism through developing novel nano-instrumentation and quantitative analysis tools for researchers and practitioners in health science directly related to the PRARP's mission.

The PIs have obtained significant preliminary data to support the proposed research hypothesis. The data was based on 24 human CSF samples from Ohio State University (OSU) brain bank. To illustrate how the data is correlated with the proposed research, we will start with a quick review of the literature data. Recent studies indicate that CSF from AD subjects show clear morphological aggregation and changes in shape among Aß peptides and tau proteins along different stages. Mechanical properties of aggregates made of Aß peptides and tau proteins are closely associated with the self-assembly status, such as fibrillization, as well as disease progression. Although the Aß peptides and tau proteins counts very small part of the overall CSF, they are believed to be directly involved into the aggregation of proteins and the formation of fibrillar structures causing neuron degeneration. Our experimental studies concluded that the changes and correlationscan be more precisely quantified using material properties (Young modulus, size, shape, concentration and distribution) of the CSF components, and as such could potentially be used as biomarkers for AD diagnosis. For AD pertaining TBI, the data may be used to draw effects of TBI to AD by comparing with patient without TBI. Quantifying micro-/nano-morphology and nano-mechanics of CSF components in a time-dependent manner relevant to AD progression may pave a new way for AD diagnosis, and understanding the effects of mechanics at the cellular level. The proposed approach can be performed rapidly with limited amounts of samples, providing a cost-effective diagnosis of AD. As shown in Fig. 5, this research team has utilize their combined expertise and experience on nano-characterization and AD clinical progression to quantify the changes of CSF components in healthy, mild, moderate, and severe AD stages. A Kalman filter-based (KF) mathematical model for evaluating individual subject's disease state, progression, and risk has been developed. The combined nanoinstrumentation platform includes an atomic force microscope (AFM), and a high-contract micro-particle imaging system (HMI). This research team has used an HMI to characterize distribution and concentration of Aß42 and tau protein aggregates from AD CSF samples. Nano-morphology and nano-mechanics of the isolated CSF components have also been characterized using AFM. Through this proposed research, the team will focus on the CSF samples to subjects resulted directly from TBI (samples will be obtained from OSU TBI clinic), and obtain statistically significant specific information to validate the research hypothesis, and build a framework for potential clinical applications.

2. A Scalable Platform for Simultaneous Analysis of Dynamic Response of Multiple Single Neuron Cells and Genes under Electrical Stimulation (Air Force Office of Scientific Research)

The goal of this research is develop and validate a scalable experimental platform that can be used for investigating responses of multiple single neuron cells or genes stimulated by controllable electrical currents/fields. The ultimate goal of this research to automate the scalable platform for high throughput screening of stimulation responses of large amounts of single neuron cells, molecules, or genes under controllable electrical fields, and build correlations of phenotypes and genotypes of cognitive relevant neuron cells, proteins, or genes for improving human performance in battle fields. The prototype platform development will serve as a pilot study for the above long-term goal. Three fundamental scientific questions to be addressed in this research are:

(1). Which molecules, proteins, or neurons in brains have the most significant effects for situation awareness or cognitive performance improvement through electrical current stimulation?
(2). What are the genes underlying the neuron cells or molecules that may contribute directly to the simulation effects?
(3). How to control the responses of either cells or genes through external stimulation, such as electrical or optical effects, so that the best human cognitive performance can be achieved?

The above are widely open scientific questions. It is very difficult to answer them through a single study. This research team asks the question: what is the best research strategy to achieve the above long-term goal? We believe a pilot study as proposed is necessary.

Our strategy is to first build a scalable experimental platform (Fig. 6), and validate the feasibility of the platform for automated high throughput screening by choosing selective molecules, proteins, neurons or genes. The goal is to test feasibility of the overall idea, and prepare for large-scale high throughput study at the second phase.

References

1. Kitazawa, K. et al. ß-Galactosyl Yariv Reagent Binds to the ß-1, 3- Galactan of Arabinogalactan Proteins. Plant Physiol. 161, 1117-1126 (2013).
2. Showalter, A. Arabinogalactan-proteins: structure, expression and function. Cell. Mol. Life Sci. 58, 1399-1417 (2001).
3. Sardar, H. S., Yang, J. & Showalter, A. M. Molecular interactions of arabinogalactan proteins with cortical microtubules and

F-actin in Bright Yellow-2 tobacco cultured cells. Plant Physiol. 142, 1469-1479 (2006).
4. Xu, J., Tan, L., Goodrum, K. J. & Kieliszewski, M. J. High-yields and extended serum half-life of human interferon a2b expressed in tobacco cells as arabinogalactan-protein fusions. Biotechnol. Bioeng. 97, 997-1008 (2007).
5. Zhang, H. et al. Mussel-inspired hyperbranched poly (amino ester) polymer as strong wet tissue adhesive. Biomaterials 35, 711-719 (2014).
6. Mehdizadeh, M., Weng, H., Gyawali, D., Tang, L. & Yang, J. Injectable citrate-based mussel-inspired tissue bioadhesives with high wet strength for sutureless wound closure. Biomaterials 33, 7972-7983 (2012).
7. Xie, D. et al. Development of injectable citrate-based bioadhesive bone implants. Journal of Materials Chemistry B 3, 387-398 (2015).
8. Flynn, T. C. & Ma, J. Theoretical Analysis of Twist/Bend Ratio and Mechanical Moduli of Bacterial Flagellar Hook and Filament. Biophysical Journal 86, 3204-3210 (2004).

Please see the attachment for diagrams and figures referred above.

Technology Transfer

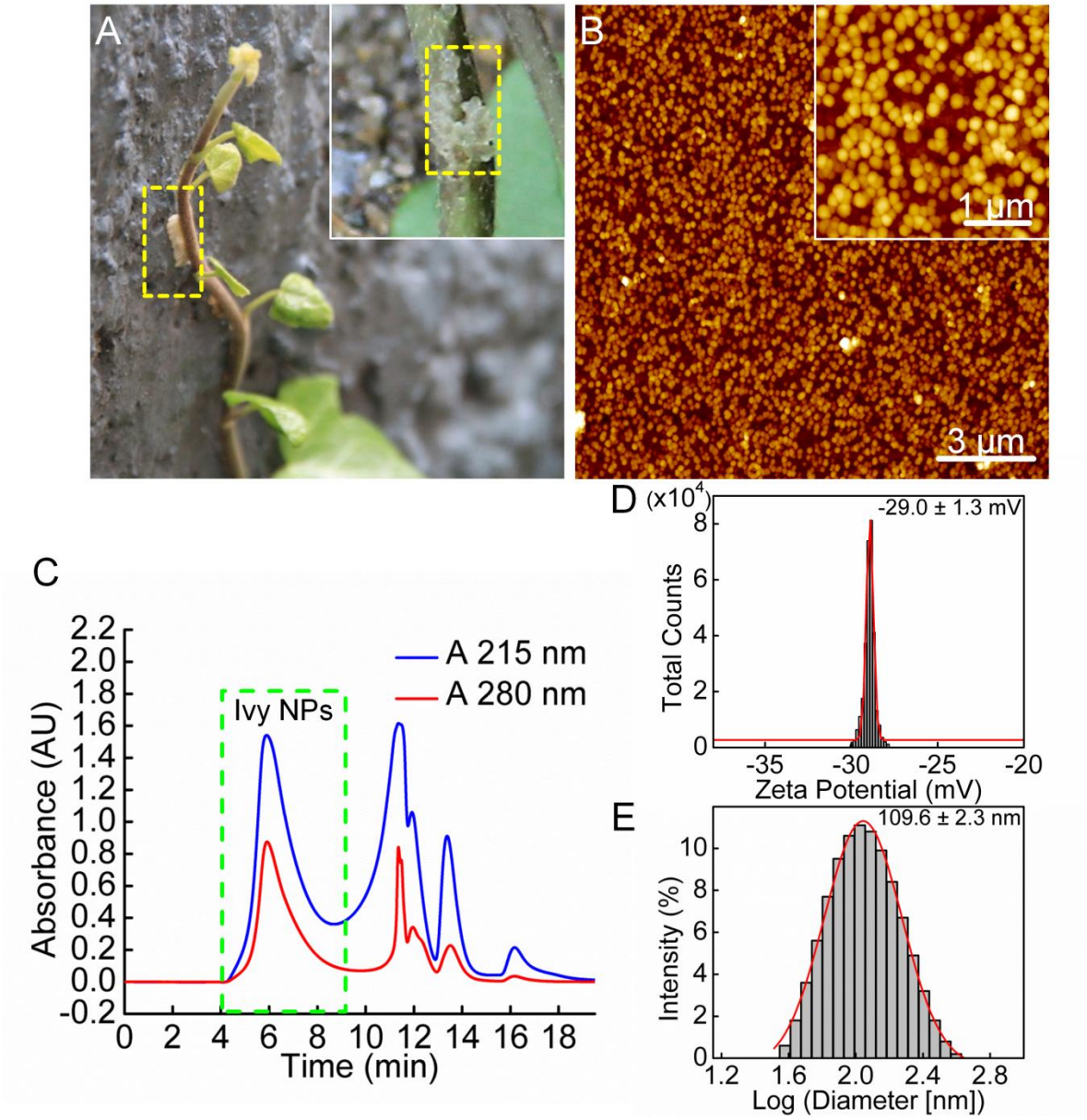

Figure 1: Characterization of nanoparticles isolated from the adventitious roots of English ivy. (**A**) Ivy shoots attached to the wall. Inset, adhesive pads formed on the adventitious roots. (**B**) AFM images of the purified ivy nanoparticles. Inset, high magnification view. Scale bars represent 3 µm and 1 µm, respectively. (**C**) SEC profiles of root extracts prepared via sonication and filtration. The first major fraction was collected and lyophilized for microscopic imaging and further chemical identification. (**D**) Zeta potential of the purified ivy nanoparticles dispersed in suspension. (**E**) Size distribution of the purified ivy nanoparticles in aqueous suspension.

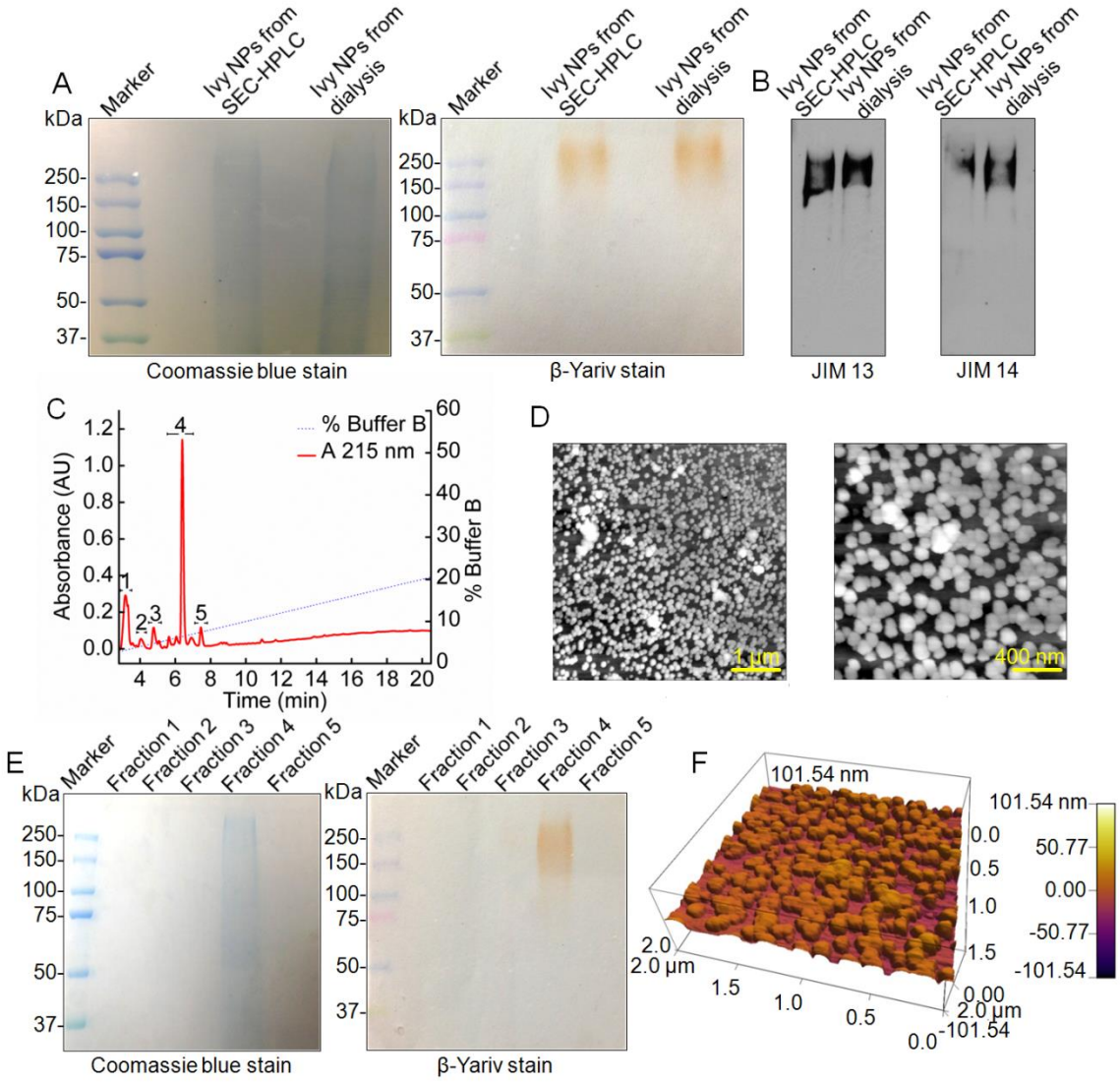

Figure 2: Chemical identification of the purified ivy nanoparticles**.** (**A**) 10% (w/v) SDS-PAGE analysis of the ivy nanoparticles purified via two methods (either SEC or dialysis as described in Methods). (**B**) Western blotting analysis of the purified ivy nanoparticles. (**C**) RP-HPLC profile of the ivy nanoparticles purified by SEC-HPLC. (**D**) AFM images of the fraction 4 obtained from RP-HPLC. Scale bars are 1 μm (left panel) and 400 nm (right panel), respectively. (**E**) Fractions 2-5, obtained from RP-HPLC, were examined by 10% (w/v) SDS-PAGE (30 ug per lane). (**F**) 3-D AFM image of fraction 4 obtained from RP-HPLC.

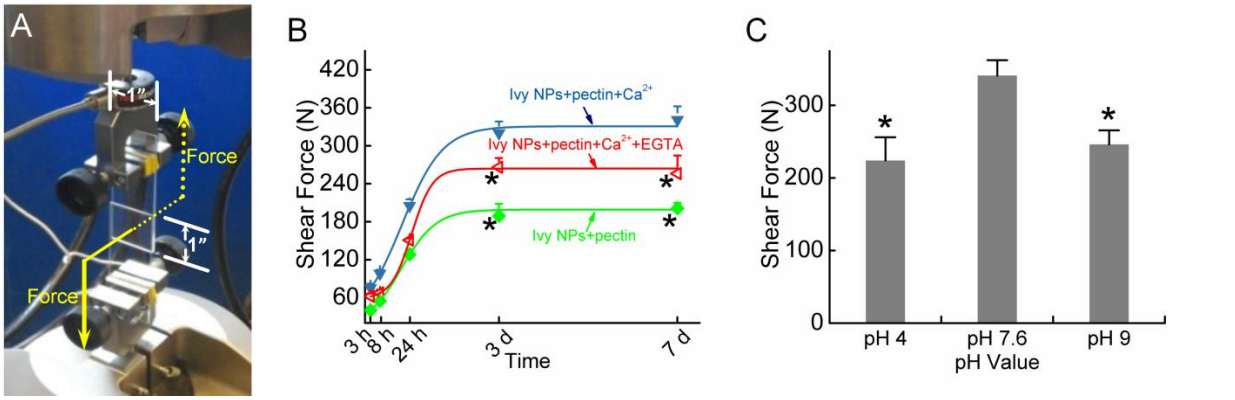

Figure 3: Adhesive lap joint shear force measurements. (**A**) Reconstructed adhesive was maintained in a 1" × 1" overlapping area of two glass slides. (**B**) Lap shear forces of the reconstructed adhesive at 3 h, 8 h, 24 h, 3 days, and 7 days. The adhesion forces of the adhesive containing chelating agent EGTA and the adhesive prepared in the absence of $CaCl_2$ were also measured at a series of time points. The force curves were fitted by OriginPro 8.0 using a growth/sigmoidal function ($y = \frac{A2 - A1}{1 + 10^{(LOGx0 - x)\,p}} + A1$). Error bars indicate SD. Significant differences between sample means are indicated: $*P < 0.05$, versus the adhesion force of the EGTA-free adhesive in the presence of calcium ions. (**C**) Influence of pH value on the adhesion forces of the reconstructed adhesive. Error bars represent SD. $*P < 0.05$, versus the adhesion force of the reconstructed adhesive prepared at pH 7.6.

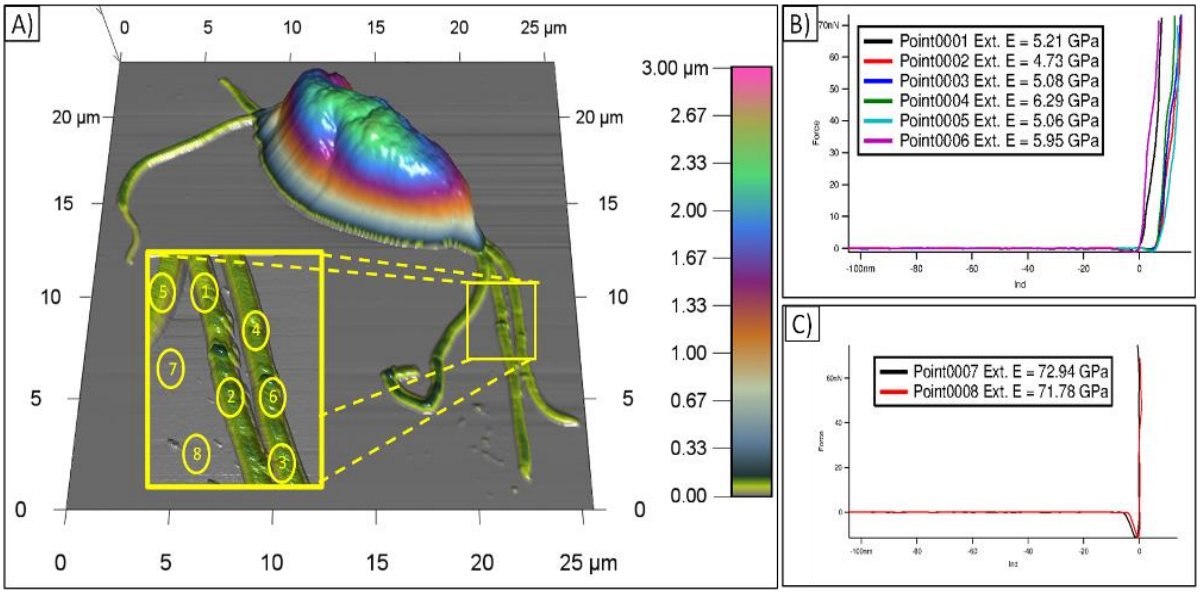

Figure 4: AFM imaging and indentation of *T. foetus* flagella. (**A**) AFM micrograph of *T. foetus* showing three anterior flagella and single posterior flagella. The color scale indicates the height in Z. The inset shows a higher magnification scan of the illustrated region, and the points indicate the location of force curves. (**B**) Force vs. indentation curves for points 1-6 showing the elastic modulus of the flagella. (**C**) Force vs. Indentation curves for points 7-8 showing the modulus of bare glass.

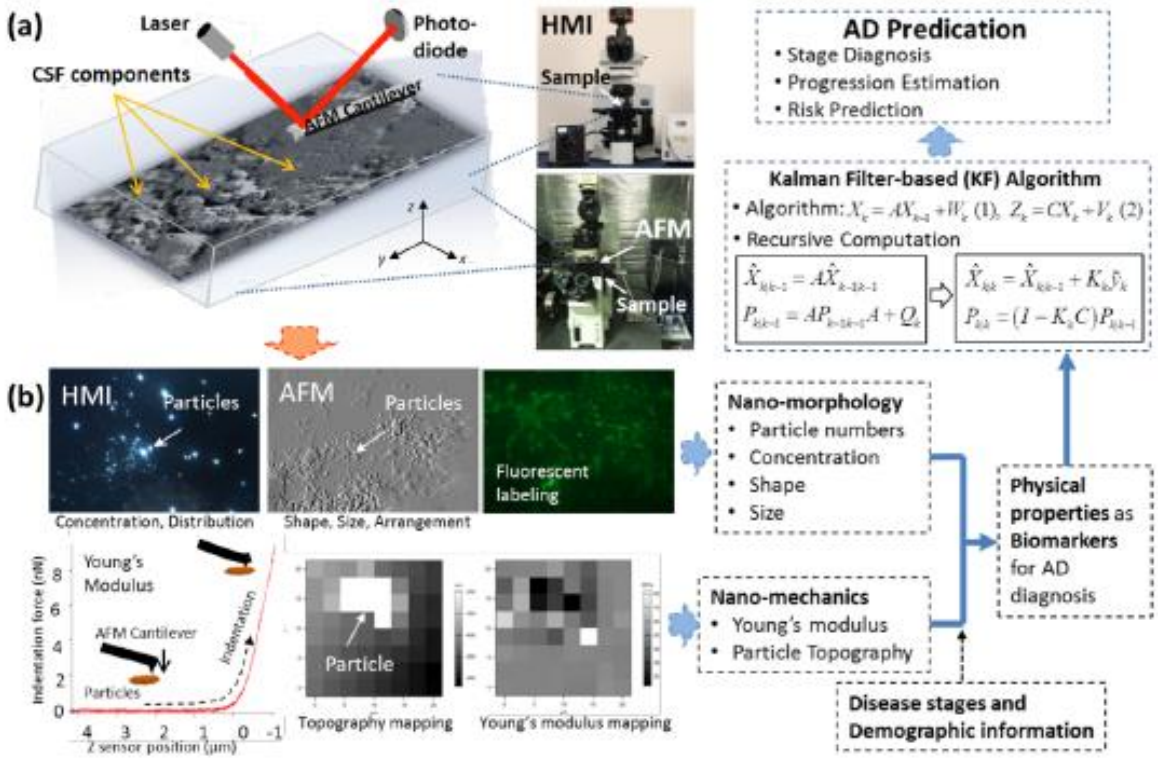

Figure 5: A combined AFM and HMI platform for nano-morphology and nano-mechanics characterization of CSF components. (**A**) Schematic drawing of the characterization platform. (**B**) Flowchart of the overall research, including characterization, extraction of physical properties extraction and Kalman Filter-based prediction.

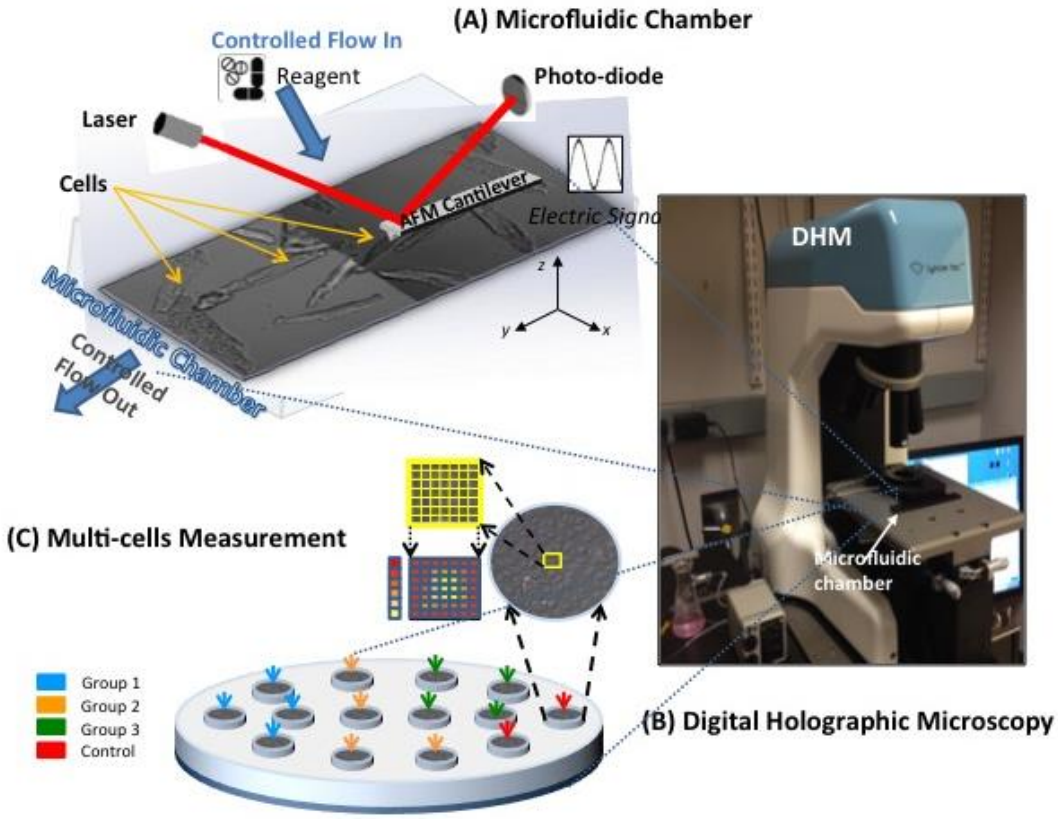

Figure 6: An MEMS integrated DHM platform for multiple single cells or molecules screening for responses under electrical current stimulation.